Science Author Reprints and Color Reimbursement

Administered and Produced by The Sheridan Press
Cindy Eyler, Reprint Customer Service Rep
The Sheridan Press, 450 Fame Avenue, Hanover, PA 17331
(800) 635-7181 ext. # 8008, (717) 632-3535, or fax (717) 633-8929 cindy.eyler@sheridan.com

Order reprints and pay color figure charges online at www.sheridan.com/aaas/eoc

Dear Author:
Science has a combined online form for ordering reprints and paying charges on color figures. You will need to use this form to pay for or receive an invoice for your color figure charges. To start your order, you'll need to enter the last seven digits of the DOI of your paper (this is a 7-digit number at the end of the references of your paper). After filling out the order form, an email will be sent for your records. An invoice will be sent with the reprints. You can pay at the time of your order, indicate that you have a purchase order, or ask to be billed.

Reimbursement for Use of Color in Science

As stated in Information for Contributors and your acceptance letter, authors requesting the use of color are required to pay $650 for the first color figure and $450 for each additional figure to help defray costs related to publishing color in the *Science* issue. **These charges are not related to your reprint order**, but are billed on the same form. Authors of solicited Reviews, Special Issue Perspectives, and Special Issue Reviews are exempt from these charges.

Printed Reprints

Author reprints must be used solely for the author's personal use. If commercial or for-profit use is intended, please contact Rockwater, Inc. at brocheleau@rockwaterinc.com or (803) 359-4578.

Only one invoice will be issued for group orders to multiple locations. Additional order forms may be obtained by contacting The Sheridan Press. **All orders must be received within 60 days of publication date or additional charges will apply.**

Prepayment or an institution purchase order is required to process your order. The online form will provide an invoice.

Delivery
Your order will be shipped within 3 weeks of the *Science* issue date. Allow extra time for delivery. If quicker delivery is necessary, please call for pricing and availability. UPS ground postage and handling are included in the prices (1-5 day delivery). Orders shipped to authors outside the continental US are mailed via an expedited air service at an additional charge. Orders for articles over 1 year past publication will require additional time to produce.

Corrections
If a serious error occurs in the published version of the paper, the error can be corrected in reprints if the editorial office is notified promptly. Please contact the editor or copy editor of your paper with the corrections.

Reprint Order Specifications
All reprints will include either a title page (in black and white or color, depending upon the type of reprint ordered) or the cover of *Science* from the issue in which your article appears. If the cover of *Science* is selected, there will be a $100 additional fee (cover will appear in black & white or color, depending on the type of reprints ordered). This adds one page to the length of your paper.

Pricing
Reprint pricing is shown in the following tables. Orders are limited to 500 copies per author. To convert color articles to black & white reprints, add $200. For articles over 12 months past publication, please contact The Sheridan Press for pricing. **This pricing is valid within 60 days of publication date.**

Black and White Reprints

Quantity	100	200	300	400	500
≤4 pages	300	350	395	435	470
≤8 pages	460	520	575	625	670
≤12 pages	600	665	725	780	830

Color Reprints

Quantity	100	200	300	400	500
≤4 pages	1800	1890	1960	2020	2070
≤8 pages	2140	2235	2310	2375	2430
≤12 pages	2485	2585	2665	2735	2795

Air Shipping Charges
(orders shipped outside the continental US only)

$120 – 8 pages or less and 200 copies or less
$175 – More than 8 pages or more than 200 copies

Instructions for Handling PDF Galley Proofs

It is important that you return galley corrections within 48 hours directly to your copy editor. Please let your copy editor know immediately if there will be any delay.

Dear Author:

Thank you for publishing in *Science*. This letter explains how to mark this PDF file and transmit corrections to your galley proofs. This PDF file includes the following:

1. Instructions for ordering reprints and paying for use of color in figures (p. 1).
2. Detailed instructions for marking the proof (pp. 2-4)
3. Galley proofs of your paper (starting on p. 5).

If your manuscript contains color figures, the colors and resolution in the proofs may appear different from those of the final published figures. Our art department will send separate color figure proofs. Also, although your paper begins at the top of a page in the proofs, it may not when printed in *Science*.

A separate PDF file showing editorial changes to your paper has been, or shortly will be, e-mailed to you by your copy editor. Please use this in checking your proofs, but do not mark corrections on it.

In order to make galley corrections:

1. Please pay color figure charges online at www.sheridan.com/aaas/eoc. The same online form can be used to order reprints.
2. Mark all changes on the galley proofs (this file) directly using Acrobat Reader (free) v. X (available at: http://get.adobe.com/reader/).
3. Additional instructions for marking text are given on the next two pages. To start, select the Comment button on the upper right side of the Adobe Reader screen.
    a. All edits of the text and text corrections should be made with "Text Edits" using insert, replace, or delete/cross out selections. *Please do not use sticky notes, comments, or other tools for actual text edits*.
    b. You can control formatting (e.g., italics or bold) by selecting edited text.
    c. Indicate edits to special or Greek characters with a comment. Use the "sticky note" for comments. Please refrain from using other tools.
    d. Please collect all corrections into one file; import comments provided by multiple authors into one file only (Document menu/Comments/Import Comments).
    e. Be sure to save the marked file and keep a copy.
4. Respond to all of the copy editor's queries listed at the end of the edited manuscript or as embedded PDF notes in the copyedited manuscript, by directly editing the galley text in the PDF with the annotation tools or using sticky notes on the galley PDF.
5. Check reference titles and additional supplementary references on the edited word file sent to you by your copyeditor. Address any edits here in the note back to your copyeditor.
6. Check all equations, special characters, and tables carefully. Check spelling of all author names for accuracy.
7. Make a copy of the corrected galley proofs for yourself. Return the corrected galley proofs to the *Science* copy editor as an attachment to an email.
8. If you cannot mark the proofs electronically, please e-mail a list of corrections to the copy editor.

Thank you for your prompt attention,
The Editors

Headquarters
1200 New York Avenue, NW Washington, DC 20005 USA Telephone: (+1) 202-326-6550 Fax (+1) 202-789-4669
Europe Office
Bateman House, 82-88 Hills road, Cambridge CB2 1LQ, UK Telephone: (+44) 1223-326500 Fax: (+44) 1223 326501
Published by the American Association for the Advancement of Science

Instructions on how to annotate your galley PDF file using Adobe Acrobat Reader X

To view, annotate and print your galley, you will need Adobe Reader X. This free software can be downloaded from: http://get.adobe.com/reader/. It is available for Windows, Mac, LINUX, SOLARIS, and Android. The system requirements can also be found at this URL.

To make corrections and annotations in your galley PDF with Adobe Reader X, use the commenting tools feature, located by clicking **Comment** at the upper right of your screen. You should then see the Annotations Palette with the following annotation tools. (These tools can also be accessed through View>Comment>Annotations.

Although all the files from SPI will have these commenting tools available, occasionally this feature will not be enabled on a particular PDF. In these cases, you can use the two default commenting tools to annotate your files: Sticky Note and Highlight Text.

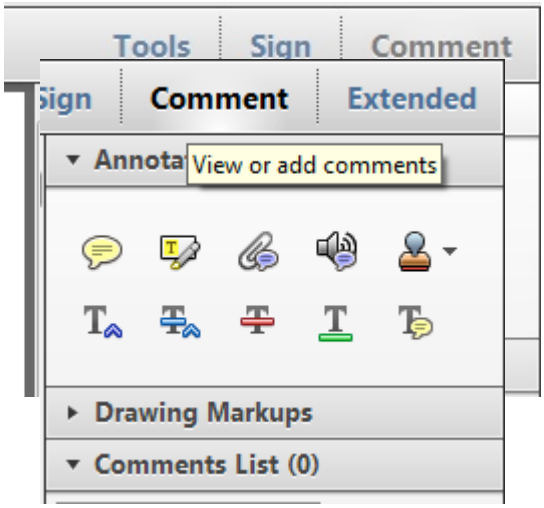

To start adding comments, select the appropriate commenting tool from the Annotation Palette.

TO INDICATE INSERT, REPLACE, OR REMOVE TEXTS

- **Insert Text**

  Click the  button on the Commenting Palette. Click to set the cursor location in the text and start typing. The text will appear in a commenting box. You may also cut-and-paste text from another file into the commenting box.
- **Replace Text**

  Click the  button on the Commenting Palette. To highlight the text to be replaced, click and drag the cursor over the text. Then type in the replacement text. The replacement text will appear in a commenting box. You may also cut-and-paste text from another file into this box.
- **Remove Text**

  Click the  button on the Commenting Palette. Click and drag over the text to be deleted. The text to be deleted will then emphasize with a ~~strikethrough~~.

LEAVE A NOTE / COMMENT

- **Add Note to Text**

Click the  button on the Commenting Palette. Click to set the location of the note on the document and simply start typing. Kindly refrain from using this feature to make text edits

- **Add Sticky Note**

Click the  button on the Commenting Palette. Click to set the location of the note on the document and simply start typing. Kindly refrain from using this feature to make text edits

HIGHLIGHT TEXT / MAKE A COMMENT

- Click the  button on the Commenting Palette. Click and drag over the text. To make a comment, double click on the highlighted text and simply start typing.

REVIEW

All comments added in the active document are listed in **Comments List** Palette. Navigate by clicking on a correction in the list.

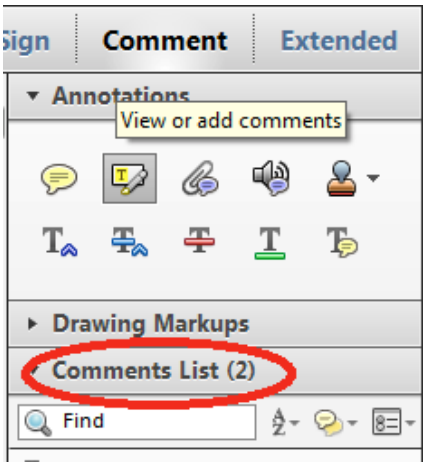

ATTACH A FILE

For equations, tables and figures that need to be added or replaced, or for a large section of text that needs to be inserted, users will find it better to just attach a file.

Click  button on the Commenting Palette. And then click on the figure, table or formatted text to be replaced. A window will automatically open allowing you to attach the file.

REPORT

SOLAR CELLS

A mixed-cation lead mixed-halide perovskite absorber for tandem solar cells

David P. McMeekin,[1] Golnaz Sadoughi,[1] Waqaas Rehman,[1] Giles E. Eperon,[1] Michael Saliba,[1] Maximilian T. Hörantner,[1] Amir Haghighirad,[1] Nobuya Sakai,[1] Lars Korte,[2] Bernd Rech,[2] Michael B. Johnston,[1] Laura M. Herz,[1] Henry J. Snaith[1]*

Metal halide perovskite photovoltaic cells could potentially boost the efficiency of commercial silicon photovoltaic modules from ~ 20 toward 30% when used in tandem architectures. An optimum perovskite cell optical band gap of ~1.75 electron volts (eV) can be achieved by varying halide composition, but to date, such materials have had poor photostability and thermal stability. Here we present a highly crystalline and compositionally photostable material, $[HC(NH_2)_2]_{0.83}Cs_{0.17}Pb(I_{0.6}Br_{0.4})_3$, with an optical band gap of ~1.74 eV, and we fabricated perovskite cells that reached open-circuit voltages of 1.2 volts and power conversion efficiency of over 17% on small areas and 14.7% on 0.715 cm^2 cells. By combining this material with a 19%-efficient silicon cell, we demonstrated the feasibility of achieving >25%-efficient four-terminal tandem cells.

One concept for improving the efficiency of photovoltaics (PVs) is to create a "tandem junction"; for example, by placing a wide–band-gap "top cell" above a silicon (Si) "bottom cell." This approach could realistically increase the efficiency of the Si cell from 25.6 to beyond 30% (*1*, *2*). Given the crystalline Si band gap of 1.1 eV, the top cell material requires a band gap of ~1.75 eV in order to current-match both junctions (*3*). However, suitable wide–band-gap top-cell materials for Si or thin-film technologies that offer stability, high performance, and low cost have been lacking. In recent years, metal halide perovskite–based PVs have gained attention because of their high power conversion efficiencies (PCEs) and low processing cost (*4*–*11*). An attractive feature of this material is the ability to tune its band gap from 1.48 to 2.3 eV (*12*, *13*), implying that we could potentially fabricate an ideal material for tandem cell applications.

Perovskite-based PVs are generally fabricated with organic-inorganic trihalide perovskites with the formulation ABX_3, where A is the methylammonium (CH_3NH_3) (MA) or formamidinium ($[HC(NH_2)_2]$) (FA) cation, B is commonly lead (Pb), and X is a halide (Cl, Br, or I). Although these perovskite structures offer high PCEs, reaching >20% PCE with band gaps of around 1.5 eV (*14*), fundamental issues have been discovered when attempting to tune their band gaps to the optimum 1.7- to 1.8-eV range. In the case of $MAPb[I(1-x)Br_x]_3$, Hoke *et al.* reported that soaking it with light induces a halide segregation within the perovskite (*15*). The formation of iodide-rich domains with a lower band gap results in an increase in sub-gap absorption and a red shift of photoluminescence (PL). The lower–band-gap regions limit the voltage attainable with such a material, so this band-gap "photoinstability" limits the use of $MAPb[I(1-x)Br_x]_3$ in tandem devices (*15*). In addition, when considering real-world applications, $MAPbI_3$ is inherently thermally unstable at 85°C, even in an inert atmosphere (international regulations require a commercial PV product to withstand this temperature) (*16*).

Concerning the more thermally stable $FAPbX_3$ perovskite, an increase in optical band gap has not resulted in an expected increase in xxxxxx xxxxx xxxxx (V_{OC}) (*13*). Furthermore, as iodide is substituted with bromide, a crystal phase transition occurs from a trigonal to a cubic structure; in compositions near the transition, the material is unable to crystallize, resulting in an apparently "amorphous" phase with high levels of energetic disorder and unexpectedly low absorption. These compositions additionally have much lower charge-carrier mobilities in the range of 1 $cm^2 V^{-1} s^{-1}$, in comparison to >20 $cm^2 V^{-1} s^{-1}$ in the neat iodide perovskite (*17*). For tandem applications, these problems arise at the Br composition needed to form the desired top-cell band gap of ~1.7 to 1.8 eV.

Nevertheless, perovskite/Si tandem PVs have already been reported in four-terminal (*18*, *19*) and two-terminal (*20*) architectures. However, their reported efficiencies have yet to surpass the optimized single-junction efficiencies, in part because of non-ideal absorber band gaps. It is possible to form a lower–band-gap triiodide perovskite material and current-match the top and bottom junctions in a monolithic architecture by simply reducing the thickness of the top cell. However, this method results in non-ideal efficiency.

Here we address the issues of forming a photostable FA-based perovskite with the ideal band gap for tandem PVs. We partially substituted the formamidinium cation with Cs and observed that the phase instability region was entirely eliminated in the iodide-to-bromide compositional range, delivering complete tunability of the band gap around 1.75 eV. We fabricated planar heterojunction perovskite PVs, demonstrating PCE of >17% and stabilized power output (SPO) of 16%. To demonstrate the potential impact of this new perovskite material in tandem solar cells, we created a semi-transparent perovskite device and measured the performance of a silicon PV after "filtering" the sunlight through the perovskite top cell. The Si cells delivered an efficiency boost of 7.3%, indicating the feasibility of achieving >25%-efficient perovskite/Si tandem cells.

The A-site cations that could be used with lead halides to form suitable perovskites for PVs are Cs, MA, and FA. $CsPbI_3$ does form a "black phase" perovskite with a band gap of 1.73 eV, but this appropriate phase is only stable at temperatures above 200° to 300°C, and the most stable phase at room temperature is a nonperovskite orthorhombic "yellow" phase. MA-based perovskites are thermally unstable and suffer from halide segregation instabilities, and are thus likely to be unsuitable (*16*). FA-based perovskites are the most likely to deliver the best balance between structural and thermal stability (*13*, *21*–*25*). However, in Fig. 1A, we show photographs of a series of $FAPb[I(1-x)Br_x]_3$ films; we observed a "yellowing" of the films for compositions of x between 0.3 and 0.6, which is consistent with the previously reported phase instability caused by a transition from a trigonal ($x < 0.3$) to a cubic ($x > 0.5$) structure (*13*). F1

We have previously observed that the band gap changes from 1.48 eV for $FAPbI_3$ to 1.73 eV for $CsPbI_3$ (*13*). Recently it has been shown that mixing Cs with FA or MA results in a slight widening of the band gap (*26*, *27*). We considered the possibility that if we partially substituted FA for Cs, we could push this region of structural instability in the Br–to-I phase space to higher energies, and thus potentially achieve a structurally stable mixed-halide perovskite with a band gap of 1.75 eV. In Fig. 1B, we show photographs of thin films fabricated from mixed-cation lead mixed-halide $FA_{0.83}Cs_{0.17}Pb(I_{(1-x)}Br_x)_3$ compositions. Unexpectedly, we did not simply shift the region of structural instability to higher energy, but we observed a continuous series of dark films throughout this entire compositional range. To confirm these observations, we also performed ultraviolet-visible absorption measurements. We obtained a sharp optical band edge for all compositions of the $FA_{0.83}Cs_{0.17}Pb(I_{(1-x)}Br_x)_3$ material (Fig. 1, C and D), in contrast to $FAPb(I_{(1-x)}Br_x)_3$, which shows weak absorption in the intermediate range.

In order to understand the impact of adding Cs upon the crystallization of the perovskite, we performed x-ray diffraction (XRD) on the series of films covering the I–to-Br compositional range. In Fig. 1E,

[1]Clarendon Laboratory, University of Oxford, Parks Road, Oxford OX1 3PU, UK. [2]Helmholtz-Zentrum Berlin für Materialien und Energie, Institute for Silicon Photovoltaics, Kekuléstrasse 5, 12489 Berlin, Germany.
*Corresponding author. E-mail: henry.snaith@physics.ox.ac.uk

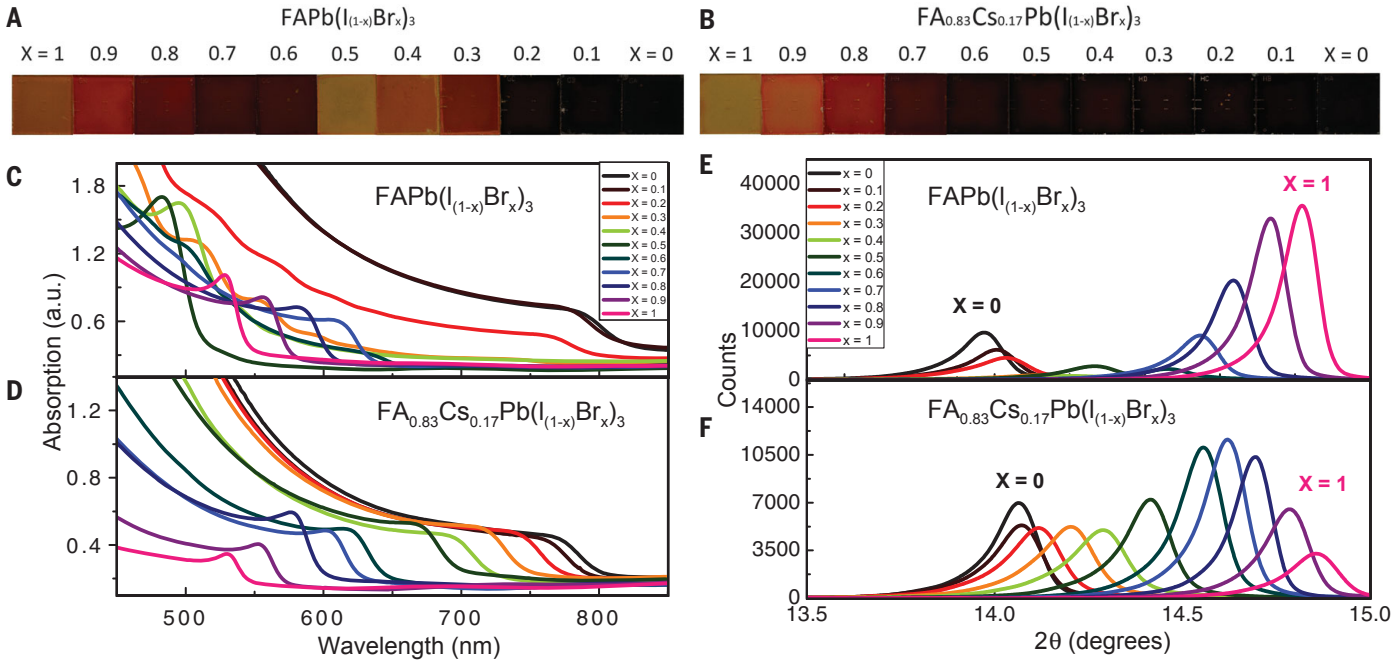

Fig. 1. Tuning the band gap. Photographs of perovskite films with Br composition increasing from x = 0 to 1 for (**A**) $FAPb(I_{(1-x)}Br_x)_3$ and (**B**) $FA_{0.83}Cs_{0.17}Pb(I_{(1-x)}Br_x)_3$. (**C**) Ultraviolet-visible absorbance spectra of films of $FAPb(I_{(1-x)}Br_x)_3$ and (**D**) $FA_{0.83}Cs_{0.17}Pb(I_{(1-x)}Br_x)_3$. a.u., arbitrary units. (**E**) (XRD pattern of $FAPb(I_{(1-x)}Br_x)_3$ and (**F**) $FA_{0.83}Cs_{0.17}Pb(I_{(1-x)}Br_x)_3$. The stated compositions are the fractional compositions of the ions in the starting solution, and the actual composition of the crystallized films may vary slightly.

we show the XRD patterns for $FAPb(I_{(1-x)}Br_x)_3$, zoomed in to the peak around 2θ ~ 14° [the complete diffraction pattern is shown in fig. S1, along with more details on fitting this data (*28*)]. For the $FA_{0.83}Cs_{0.17}Pb(I_{(1-x)}Br_x)_3$ perovskite, the material is in a single phase throughout the entire composition range. The monotonic shift of the (100) reflection that we observed from 2θ ~ 14.2° to 14.9° is consistent with a shift of the cubic lattice constant from 6.306 to 5.955 Å as the material incorporates a larger fraction of the smaller halide, Br [in fig. S2, we show the complete diffraction pattern (*28*)]. Thus, for the $FA_{0.83}Cs_{0.17}Pb(I_{(1-x)}Br_x)_3$ perovskite, we have removed the structural phase transition and instability over the entire compositional range [in figs. S3 to S5 we show details of varying the Cs concentration and the Br–to-I concentration (*28*)]. Over the entire Br-to-I range, and for a large fraction of the Cs-FA range, the variation in lattice constant, composition, and optical band gap precisely follows Vegard's law [fig. S6 (*28*)], so we had total flexibility and predictability in tuning the composition and its impact on the band gap. For the results that follow below, we used the precise composition $FA_{0.83}Cs_{0.17}Pb(I_{0.6}Br_{0.4})_3$, which has an optical band gap of 1.74 eV as determined by a Tauc plot [fig. S7 (*28*)].

Photoinduced halide segregation has been reported in methylammonium lead mixed-halide perovskites (*15*). A red shift in PL upon light illumination, for intensities ranging from 10 to 100 mW cm^{-2} occurs, with the shift to lower energies resulting from the formation of iodine-rich domains that have lower band gaps. This limits the achievable open-circuit voltage of the solar cell device by introducing a large degree of electronic disorder. In Fig. 2, we show the PL from films of $MAPb(I_{0.6}Br_{0.4})_3$ perovskite and the mixed-cation mixed-halide material $FA_{0.83}Cs_{0.17}Pb(I_{0.6}Br_{0.4})_3$, immediately after prolonged periods of light exposure, using a power density of ~3 mW cm^{-2} and a wavelength of 550 nm as an excitation source. We confirmed the results observed by Hoke *et al.*, in which we saw a time-dependent red shift in PL for the $MAPb(I_{0.6}Br_{0.4})_3$ film, which exhibited a 130-meV PL red shift after only 1 hour of illumination. We also show the time evolution of the PL from $MAPb(I_{0.8}Br_{0.2})_3$, a composition previously reported in other devices (*29*), which shifts from 1.72 to 1.69 eV [fig. S8 (*28*)]. In contrast, although we saw a rise in PL intensity, we observed no significant red shift in PL emission for the $FA_{0.83}Cs_{0.17}Pb(I_{0.6}Br_{0.4})_3$ precursor after 1 hour of identical light illumination (which we show in Fig. 2B). Furthermore, we exposed a similar $FA_{0.83}Cs_{0.17}Pb(I_{0.6}Br_{0.4})_3$ film to monochromatic irradiance of much higher irradiance of 5 W cm^{-2} and observed no red shift after 240 s of illumination [fig. S9, (*28*)]. Under these identical conditions, we did observe a red shift in the PL for the single-cation $FAPb(I_{0.6}Br_{0.4})_3$ perovskite, as we have previously reported (*17*). In addition, under thermal stressing at 130°C, we observed that the optical band gap and the crystal lattice of $FA_{0.83}Cs_{0.17}Pb(I_{0.6}Br_{0.4})$ were stable, in contrast to those of $MAPb(I_{0.6}Br_{0.4})_3$ (fig. S10).

Beyond halide segregation, a further deleterious observation previously made for mixed-halide perovskites has been that the energetic disorder in the material is greatly increased in comparison to the neat iodide perovskites. The ultimate open-circuit voltage that a solar cell material can generate is intimately linked to the steepness of the absorption onset just below the band edge, which can be quantified by the Urbach energy (E_u) (*30*, *31*). This E_u reported by De Wolf *et al.* and Sadhanala *et al.* for $MAPbI_3$ was 15 meV (*31*), where small values of E_u indicate low levels of electronic disorder. In contrast, the E_u for $MAPb(I_{0.6}Br_{0.4})_3$ perovskite increased to 49.5 meV (*32*). We determined E_u by performing Fourier-transform photocurrent spectroscopy (FTPS) on complete planar heterojunction solar cells (details of the solar cells are discussed below), and in Fig. 2C we show the semi-log plot of external quantum efficiency (EQE) absorption edge of a device fabricated with the optimized precursor solution and annealing procedure. We calculated an E_u of 16.5 meV, which is near the values reported for the neat iodide perovskites. F2

In order to further assess the electronic quantity of $FA_{0.83}Cs_{0.17}Pb(I_{0.6}Br_{0.4})_3$, we performed optical pump terahertz-probe (OPTP) spectroscopy, which is a noncontact method of probing the photoinduced conductivity and effective charge-carrier mobility in the material. In Fig. 2D, we show the fluence dependence of the OPTP transients, which exhibit accelerated decay dynamics at higher initial photoinjected charge-carrier densities, as the result of enhanced contributions from bimolecular and Auger recombination. We may extract the rate constants associated with different recombination mechanisms by global fits to these transient of the solutions to the rate equation

$$\frac{dn(t)}{dt} = -k_3 n^3 - k_2 n^2 - k_1 n \qquad (1)$$

We found that $FA_{0.83}Cs_{0.17}Pb(I_{0.6}Br_{0.4})_3$ exhibits an excellent charge-carrier mobility of 21 $cm^2\ V^{-1}\ s^{-1}$. For comparison, the corresponding

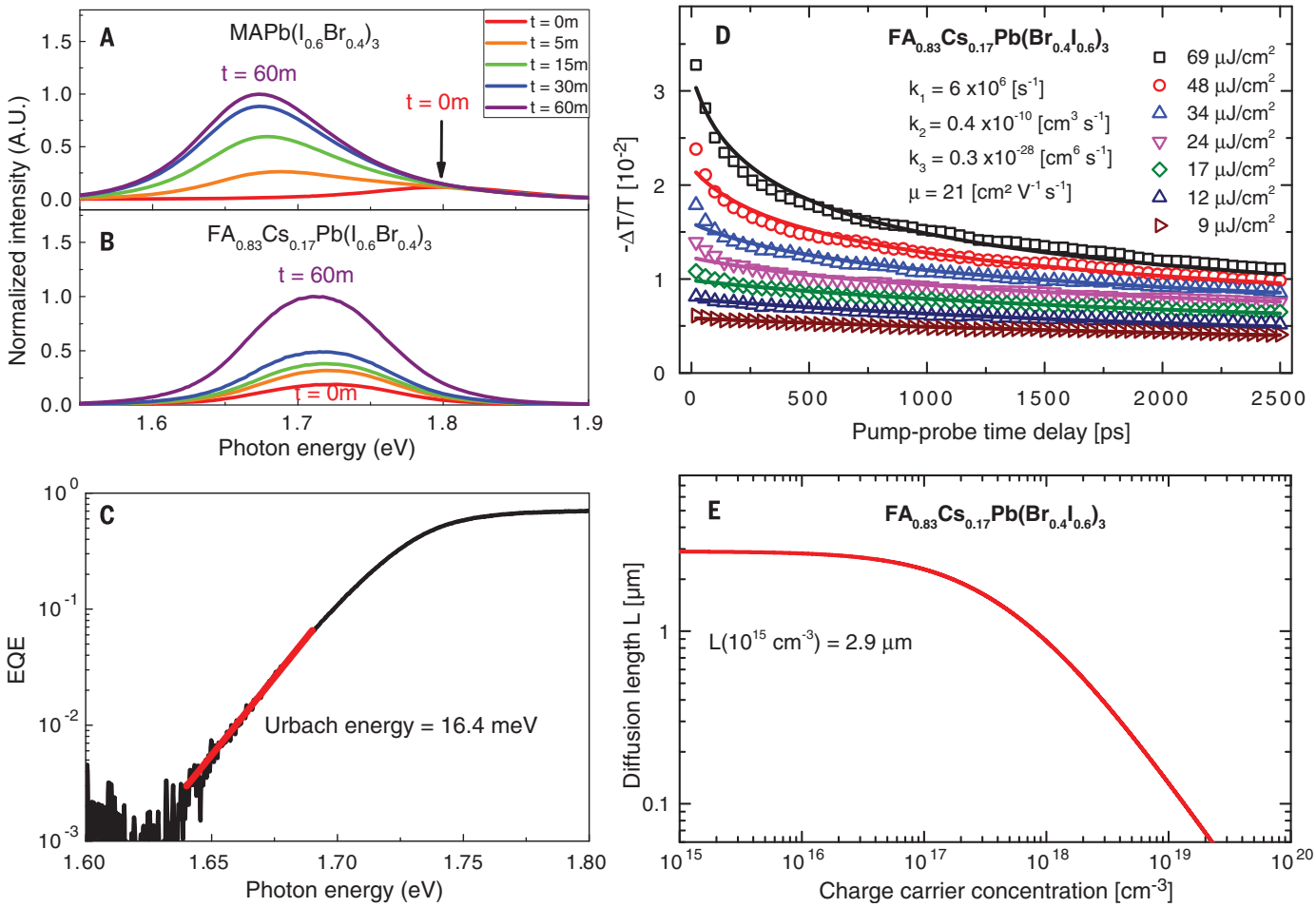

Fig. 2. Material characteristics of $FA_{0.83}Cs_{0.17}Pb(I_{0.6}Br_{0.4})_3$ perovskite. Normalized PL measurement measured after 0, 5, 15, 30, and 60 min of light exposure of the (**A**) $MAPb(I_{0.6}Br_{0.4})_3$ and (**B**) $FA_{0.83}Cs_{0.17}Pb(I_{0.6}Br_{0.4})_3$ thin films. (**C**) Semi-log plot of EQE at the absorption onset for a $FA_{0.83}Cs_{0.17}Pb(I_{0.6}Br_{0.4})_3$ PV cell, measured using FTPS at short-circuit (J_{SC}). (**D**) OPTP transients for a $FA_{0.83}Cs_{0.17}Pb(I_{0.6}Br_{0.4})_3$ thin film, measured after excitation with a 35-fs light pulse of wavelength 400 nm with different fluences. (**E**) Charge-carrier diffusion length L as a function of charge concentration.

neat FA perovskite $FAPb(I_{0.6}Br_{0.4})_3$ only sustains charge-carrier mobilities <1 $cm^2\ V^{-1}\ s^{-1}$ that are related to the amorphous and energetically disordered nature of these materials (*17*). Conversely, $FA_{0.83}Cs_{0.17}Pb(I_{0.6}Br_{0.4})_3$ displays a mobility value intermediate to those we previously determined (*17*) for $FAPbI_3$ (27 $cm^2\ V^{-1}\ s^{-1}$) and $FAPbBr_3$ (14 $cm^2\ V^{-1}\ s^{-1}$), which suggests that it is no longer limited by structural disorder. F3

We further assessed the potential of $FA_{0.83}Cs_{0.17}Pb(I_{0.6}Br_{0.4})_3$ for incorporation into planar heterojunction PV architectures by deriving the charge-carrier diffusion length $L = [\mu k_B T/(eR)]^{0.5}$ as function of the charge-carrier density n, where $R = k_1 + nk_2 + n^2k_3$ is the total recombination rate, k_B is the Boltzmann constant, T is temperature, and e is the elementary charge. In Fig. 2E, we show that for charge-carrier densities typical under solar illumination ($n \sim 10^{15}$ cm^{-3}) a value of $L \sim 2.9$ μm is reached, which is comparable to values reported for high-quality thin films of neat lead iodide perovskites (*17*, *33*). The high charge-carrier mobility and slow recombination kinetics, and the long charge carrier diffusion length, imply that this mixed-cation, mixed-halide perovskite should be just as effective as a high-quality solar cell absorber material as the neat halide perovskite $FAPbI_3$.

We fabricated a series of planar heterojunction solar cells to assess the overall solar cell performance [in fig. S11 we describe in more detail and show data for solar cells fabricated with a range of compositional and processing parameters (*28*)]. We show the device architecture in Fig. 3A, which is composed of a SnO_2/phenyl-C_{60}-butyric acid methyl ester ($PC_{60}BM$) electron-selective layer, a solid $FA_{0.83}Cs_{0.17}Pb(I_{0.6}Br_{0.4})_3$ perovskite absorber layer, and Li-TFSI–doped (TFSI, xxxxx xxxxx xxxx) spiro-OMeTAD (xxxxx xxxxx xxxxxxx xxxxxxx) with 4-tert-butylpyridine (TBP) additive as the hole-collection layer, caped with an Ag electrode. We measured current-voltage (*I-V*) characteristics of such devices under a simulated air mass (AM) 1.5, under 100 mW cm^{-2} of sunlight, and show the *I-V* characteristics of one of the highest-performing devices in Fig. 3B. It delivered a short-circuit current density of 19.4 mA cm^{-2}, a V_{OC} of 1.2 V, and a PCE of 17.1%. By holding the cell at a fixed maximum power point forward-bias voltage of 0.95 V, we measured the power output over time, reaching a stabilized efficiency of 16% (Fig. 3C). The highest jxxxxx vxxxxx (JV) efficiency we measured was 17.9% [fig. S12 (*28*), along with a histogram of performance parameters for a large batch of devices in fig. S13 (*28*)]. To demonstrate that these cells can also operate with larger area, we fabricated 0.715-cm^2 active layers in which the cells reach a stabilized power output of >14% [fig. S14 (*28*)]. In Fig. 3D, we show the spectral response of the solar cell, which confirms the wider band gap of the solar cell and also integrates over the AM 1.5 solar spectrum to give 19.2 mA cm^{-2}, in close agreement to the measured xxxxxx xxxxxxx xxxxxx (J_{SC}).

This performance is very competitive with that of the best reported single-junction perovskite solar cell reported so far (*30*, *34*), especially considering the wider band gap of our material, which should result in a few percentage points of absolute efficiency drop with respect to a 1.55-eV material (*35*). Importantly for tandem solar cells, this 1.74-eV material appears to be capable of generating a higher V_{OC} than the 1.55-eV triiodide perovskites in planar heterojunction solar cells. Following Rau *et al.* (*36*), from the integration of the EQE over the blackbody radiation

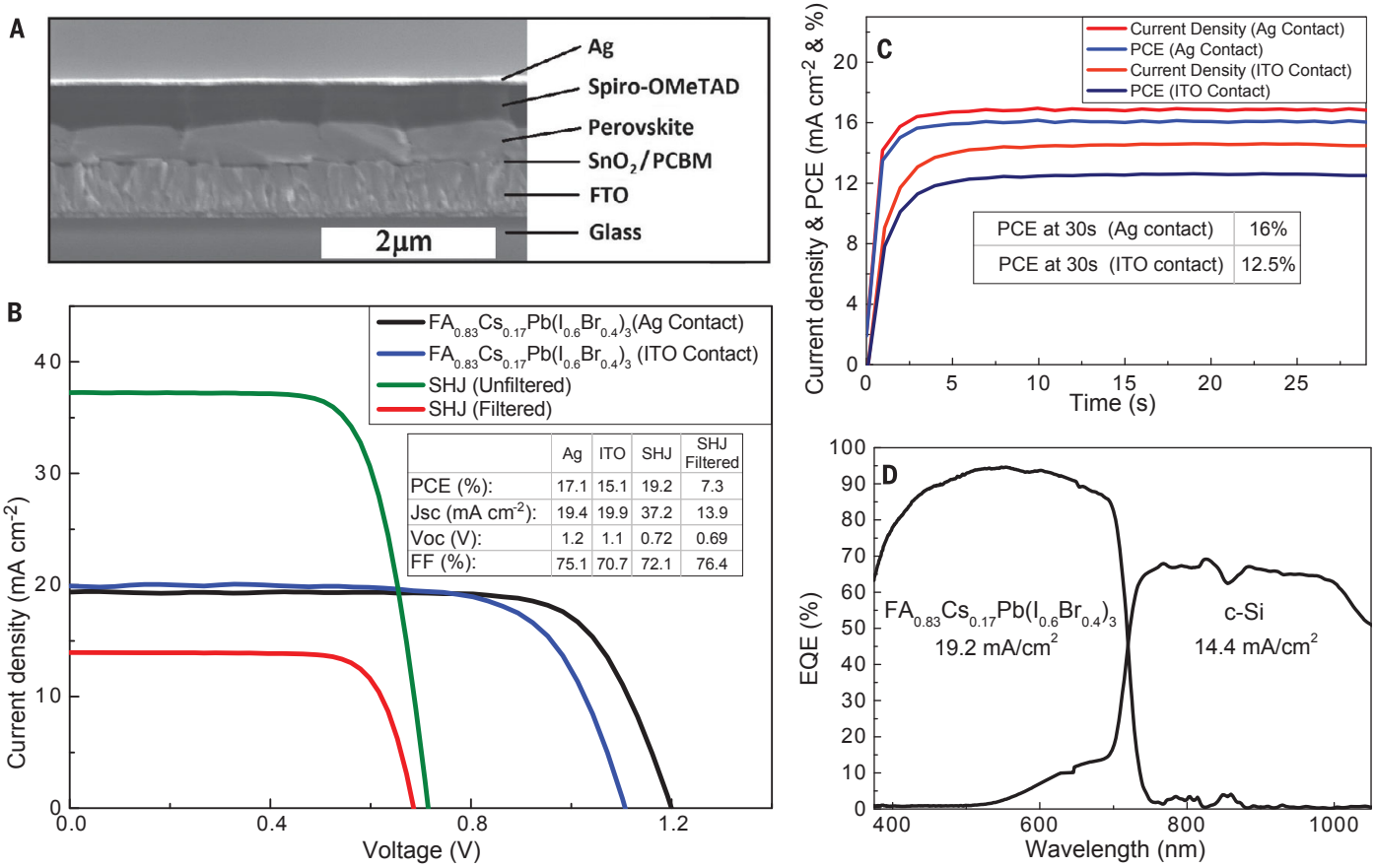

	Ag	ITO	SHJ	SHJ Filtered
PCE (%):	17.1	15.1	19.2	7.3
Jsc (mA cm^{-2}):	19.4	19.9	37.2	13.9
Voc (V):	1.2	1.1	0.72	0.69
FF (%):	75.1	70.7	72.1	76.4

Fig. 3. Device architecture and *I-V* characteristics for $FA_{0.83}Cs_{0.17}Pb(I_{0.6}Br_{0.4})_3$ perovskite and Si PV cells. (**A**) Scanning electron microscope image of a cross-section of a planar heterojunction solar cell. PCBM, pxxxx cxxxx bxxxx mxxxx. (**B**) Forward bias to short-circuit *I-V* curve for the best perovskite devices fabricated, using either a Ag metal or semi-transparent ITO top electrode, measured at a 0.38 V/s scan rate. FF, fxxxxx fxxxxx. We also show the *I-V* curve of aSHJ cell, measured with direct light or with the simulated sunlight filtered through the semi-transparent perovskite solar cell (*37*). The SHJ cells were measured at the Centre For Renewable Energy Technologies, Loughborough, UK, under an extremely well-calibrated solar simulator. (**C**) Photocurrent density and power conversion efficiency measured at the maximum power point for a 30-s time span. (**D**) EQE spectrum measured in short-circuit (J_{SC}) configuration for the highest-efficiency perovskite cell and the SHJ cell measured with the incident light filtered through the semi-transparent perovskite cell.

spectrum, we estimate the maximum attainable V_{OC} for our $FA_{0.83}Cs_{0.17}Pb(I_{0.6}Br_{0.4})_3$ device to be 1.42 V (details shown in fig. S15), which is 100 mV higher than that estimated for $MAPbI_3$ devices by Tvingstedt *et al.* and Tress *et al.* (*30*, *34*).

In order to demonstrate the potential impact of using this new perovskite composition in a tandem architecture, we fabricated semitransparent perovskite solar cells by sputter-coating ixxxx txxxx oxxxx (ITO) on top of the perovskite cells, with the additional inclusion of a thin "buffer layer" of solution-processed ITO nanoparticles between the spiro-OMeTAD and the ITO. The efficiency of the semi-transparent $FA_{0.83}Cs_{0.17}Pb(I_{0.6}Br_{0.4})_3$ solar cells is 15.1%, as determined by the *I-V* curve, with a stabilized power output of 12.5%. Because J_{SC} is similar to that of the cell with the Ag electrode, we expect that the slight drop in V_{OC} and SPO will be surmountable by better optimization of the ITO sputter-deposition procedure and buffer layer. We measured a Si heterojunction (SHJ) cell, with and without a semi-transparent perovskite cell held in front of it, and determined an efficiency of 7.3% filtered and 19.2% when uncovered. These results demonstrate the feasibility of obtaining a combined tandem solar cell efficiency ranging from 19.8%, if we combine with the stabilized power output of the semi-transparent cell, to 25.2% if we combine with the highest JV measured efficiency of the $FA_{0.83}Cs_{0.17}Pb(I_{0.6}Br_{0.4})_3$ cell. Considering further minor improvements in the perovskite, optical management and integration, and choice of Si rear cell, it is feasible that this system could deliver up to 30% efficiency. In addition, this monotonic tunability of the band gap across the visible spectrum within a single crystalline phase, will have direct impact on the color tunability and optimization of perovskites for light-emitting applications.

REFERENCES AND NOTES

1. V. Sivaram, S. D. Stranks, H. J. Snaith, *Sci. Am.* **313**, 54–59 (2015).
2. M. A. Green, K. Emery, Y. Hishikawa, W. Warta, E. D. Dunlop, *Prog. Photovolt. Res. Appl.* **23**, 805–812 (2015).
3. A. Shah, P. Torres, R. Tscharner, N. Wyrsch, H. Keppner, *Science* **285**, 692–698 (1999).
4. C. R. Kagan, D. B. Mitzi, C. D. Dimitrakopoulos, *Science* **286**, 945–947 (1999).
5. A. Kojima, K. Teshima, Y. Shirai, T. Miyasaka, *Priv. Commun.* **1**, 1 (2009).
6. M. M. Lee, J. Teuscher, T. Miyasaka, T. N. Murakami, H. J. Snaith, *Science* **338**, 643–647 (2012).
7. M. Liu, M. B. Johnston, H. J. Snaith, *Nature* **501**, 395–398 (2013).
8. J. Burschka *et al.*, *Nature* **499**, 316–319 (2013).
9. M. Green, A. Ho-Baillie, H. J. Snaith, *Nat. Photonics* **8**, 506–514 (2014).
10. N. J. Jeon *et al.*, *Nat. Mater.* **13**, 897–903 (2014).
11. N. J. Jeon *et al.*, *Nature* **517**, 476–480 (2015).
12. J. H. Noh, S. H. Im, J. H. Heo, T. N. Mandal, S. I. Seok, *Nano Lett.* **13**, 1764–1769 (2013).
13. G. E. Eperon *et al.*, *Energy Environ. Sci.* **7**, 982 (2014).
14. W. S. Yang *et al.*, *Science* **348**, 1234–1237 (2015).
15. E. T. Hoke *et al.*, *Chem. Sci.* **6**, 613–617 (2015).
16. B. Conings *et al.*, *Adv. Energy Mater.* (2015).
17. W. Rehman *et al.*, *Adv. Mater.* (2015).
18. C. D. Bailie *et al.*, *Energy Environ. Sci.* **8**, 956–963 (2015).
19. P. Löper *et al.*, *Phys. Chem. Chem. Phys.* **17**, 1619–1629 (2015).
20. S. Albrecht *et al.*, *Energy Environ. Sci.* (2015).
21. A. Binek, F. C. Hanusch, P. Docampo, T. Bein, *J. Phys. Chem. Lett.* **6**, 1249–1253 (2015).
22. S. Pang *et al.*, *Chem. Mater.* **26**, 1485–1491 (2014).
23. C. C. Stoumpos, C. D. Malliakas, M. G. Kanatzidis, *Inorg. Chem.* **52**, 9019–9038 (2013).
24. N. Pellet *et al.*, *Angew. Chem. Int. Ed. Engl.* **53**, 3151–3157 (2014).
25. S. D. Stranks, H. J. Snaith, *Nat. Nanotechnol.* **10**, 391–402 (2015).
26. J.-W. Lee *et al.*, *Adv. Energy Mater.* (2015).
27. H. Choi *et al.*, *Nano Energy* **7**, 80–85 (2014).
28. See the supplementary materials on *Science* Online.
29. C. Bi, Y. Yuan, Y. Fang, J. Huang, *Adv. Energy Mater.* (2014).

30. K. Tvingstedt *et al.*, *Sci. Rep.* **4**, 6071 (2014).
31. S. De Wolf *et al.*, *J. Phys. Chem. Lett.* **5**, 1035–1039 (2014).
32. A. Sadhanala *et al.*, *J. Phys. Chem. Lett.* **5**, 2501–2505 (2014).
33. R. L. Milot, G. E. Eperon, H. J. Snaith, M. B. Johnston, L. M. Herz, *Adv. Funct. Mater.* (2015).
34. W. Tress *et al.*, *Adv. Energy Mater.* (2014).
35. H. J. Snaith, *Adv. Funct. Mater.* **20**, 13–19 (2010).
36. U. Rau, *Phys. Rev. B* **76**, 085303 (2007).
37. L. Mazzarella *et al.*, *Appl. Phys. Lett.* **106**, 023902 (2015).

ACKNOWLEDGMENTS

This project was funded in part by the Engineering and Physical Sciences Research Council through the Supergen Solar Energy Hub SuperSolar (EP/M024881/1) and the European Research Council (EP/M014797/1) through the Stg-2011 Hybrid Photovoltaic Energy Relays and the U.S. Office of Naval Research. M.H. is funded by Oxford Pxxxxx Vxxxxx. W.R. is supported by the Hans-Boeckler-Foundation. We thank our colleagues from the Centre For Renewable Energy Technologies Photovoltaic Measurement and Testing Laboratory, Loughborough University, for their contributions to the measurements of the semi-transparent devices. We also thank K. Jacob and M. Wittig [Helmholtz-Zentrum Berlin (HZB), Institute for Silicon Photovoltaics], L. Mazzarella, and S. Kirner (HZB, Institute PVcomB) for their contributions to fabricating the SHJ cell. The University of Oxford has filed a patent related to this work. The project was designed and conceptualized by D.M. and H.J.S. D.M. performed experiments, analyzed data, and wrote the paper. G.S. fabricated and measured devices with semi-transparent electrodes. W.R. characterized the material using THz spectroscopy. G.E. helped with the experimental work and provided technical feedback on the writing of the paper. M.S. provided input and technical direction on the FA/Cs cation mixture. M.H. performed simulations for the optical modeling and calculated the maximum achievable V_{OC}. A.H. analyzed XRD data. N.S. provided input on the preparation of thin films using chemical bath depositions. L.K. and B.R. fabricated the SHJ cells. M.J. performed and analyzed EQE measurements. L.H. supervised and analyzed the THz spectroscopy measurements. H.J.S. supervised the overall conception and design of this project.

SUPPLEMENTARY MATERIALS

www.sciencemag.org/content/[volume]/[issue]/[page]/suppl/DC1
Materials and Methods
Supplementary Text
Figs. S1 to S15
References (*38–42*)

5 October 2015; accepted 3 December 2015
10.1126/science.aad5845